Proceedings of the 2001 IEEE
International Conference on Robotics & Automation
Seoul, Korea • May 21-26, 2001

Real-time 3D walking pattern generation for a biped robot with telescopic legs

Shuuji Kajita, Osamu Matsumoto and Muneharu Saigo
Mechanical Engineering Laboratory
Namiki 1-2, Tsukuba Ibaraki 305, Japan
E-mail: kajita@mel.go.jp

Abstract

Meltran V, a new biped robot with telescopic legs, is introduced. For 3D walking control of the robot we analyze the dynamics of a three-dimensional inverted pendulum in which motion is constrained to move along an arbitrarily defined plane. From this analysis we obtain simple linear dynamics, the Three-Dimensional Linear Inverted Pendulum Mode (3D-LIPM). Using a real-time control method based on 3D-LIPM, the Meltran V robot successfully demonstrated 3D dynamic walking without the use of any prepared trajectories.

1 Introduction

Research on humanoid robots and biped locomotion is currently one of the most exciting topics in the field of robotics and there exist many ongoing projects. Although some of the research has already demonstrated very reliable dynamic biped walking[5, 12], we believe it is still important to understand the theoretical background of biped locomotion and to quantitatively evaluate experimental data to achieve further advances in biped walking robots. For this reason, we developed a new biped walking robot as the platform to evaluate basic walking experiments.

The Meltran V robot has 12 joints that are sufficient for it to perform various walking maneuvers in a 3D space. Its distinctive feature is that it has telescopic legs which have some advantages over the legs with knee joints. The advantages are explained in the next section.

To get an insight into 3D walking control, we analyzed the dynamics of a three-dimensional inverted pendulum which has its motion constrained to move along an arbitrarily defined plane. From this analysis, we obtain simple linear dynamics that describe the horizontal motion of the inverted pendulum under the applied constraint. The dynamics model, the Three-Dimensional Linear Inverted Pendulum Mode (3D-LIPM), is useful because it allows a separate controller design for the sagittal (x-z) and the lateral (y-z) motion.

Using 3D-LIPM as the nominal dynamics of the Meltran V robot, we built a controller which could generate a walking pattern in real-time without using prepared joint trajectories. The results of our dynamic walking experiments are shown at the end of this report.

2 Meltran V the 12DOF biped robot

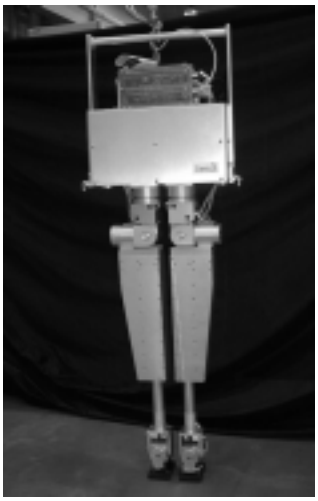

Figure 1: *Meltran V*

Meltran V is a 12DOF biped robot 1.4 m in height and weighs 46 kg. Figures 1, 2 and Table 1 give an overview of the robot. Each leg has 6DOF which is sufficient for walking in a 3D space. The hip joints (roll,

pitch, yaw) and the ankle joints (roll, pitch) are driven by brushless DC servomotors and harmonic drives. Meltran V does not have knee joints but instead has prismatic joints driven by brushless DC servomotors and ball screws. The prismatic joints can change the distance between the hip and the ankle from 0.6 to 0.9 m and the stroke is long enough for walking up typical stairs in ordinary buildings. Our ultimate goal is to develop a robot which can maneuver in almost all environments of our everyday life.

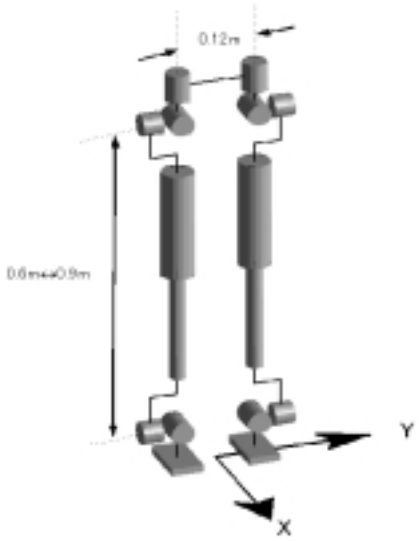

Figure 2: *Joint configulation*

There are two advantages of the telescopic legs. First, they are good for walking in a complicated environment (e.g., a power plant). Compared with a humanoid robot which bends its knees when walking, a robot with telescopic legs sweeps a smaller area. This can minimize collisions between the legs and the environment. Moreover the calculation for detecting and avoiding collisions is easy.

As the second advantage, it is easy to design a controller. This is because telescopic legs do not have singular points in the working space and have uniform manipulability. In contrast, a humanoid robot with knees suffers from singularity near full extension. (For this reason, a humanoid robot must bend its knees deeply before it starts walking.)

In the history of biped research, there have been many biped robots with telescopic legs[1, 3, 8, 11]. However, most of them were limited to two dimensional walking. Raibert and his colleagues[9] developed one of the most famous 3D bipeds with telescopic legs which demonstrated running and somersaults using powerful pneumatic actuators. Our intention, however, is to control walking in an involved environment using various sensors.

Each foot of Meltran V is equipped with a six-axis force torque sensor to enable the robot to measure all forces and moments acting from the floor. To measure the body posture and the angular velocities, three rate gyros for roll, pitch and yaw rotation and three accelerometers for x, y and z direction are embedded in the body.

All sensors and encoders of the servomotors are interfaced to an onboard computer (Pentium 200 MHz) running Realtime Linux V1.2 (http://www.rtlinux.org). The robot has power supply cables and an Ethernet cable to communicate with the host computer when we develop control programs and do data analysis.

Table 1: *Meltran V specification*

Height	1.4m
Weight	46kg
DOF	12DOF
Foot	
size	0.12m × 0.08m
material	rubber (Neopren)
6axis force sensor	*Nitta* 67M25A 50-I40
Posture sensors	
rate gyro	*Tokimec* TFG-160D ×3
accelerometer	*Tokimec* TA-25D-05 ×3
Actuators (*Minimotor*)	
leg extention	3564K 012B (109W)
hip roll, pitch & yaw	3564K 048B (101W)
ankle roll & pitch	2444S 048B (37W)

3 Derivation of 3D Linear Inverted Pendulum Mode

3.1 Motion equation of a 3D inverted pendulum

When Meltran V is supporting its body on one leg, its dominant dynamics can be represented by a single inverted pendulum which connects the supporting foot and the robot's center of gravity. Figure 3 depicts such an inverted pendulum consisting of a point mass and a massless telescopic leg. The position of the point mass $\boldsymbol{p} = (x, y, z)$ is uniquely specified by a set of state variables $\boldsymbol{q} = (\theta_r, \theta_p, r)$.

$$x = rS_p \tag{1}$$
$$y = -rS_r \tag{2}$$
$$z = rD \tag{3}$$

$$S_r \equiv \sin\theta_r, S_p \equiv \sin\theta_p, D \equiv \sqrt{1 - {S_r}^2 - {S_p}^2}$$

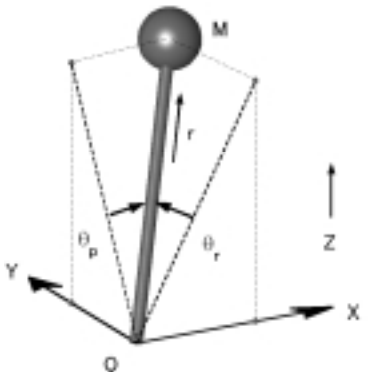

Figure 3: *3D Pendulum*

The minus sign in (2) is neccessary since we are taking right-handed coordinate system.

Let (τ_r, τ_p, f) be the actuator torque and force associated with the state variables (θ_r, θ_p, r). With these inputs, the equation of motion of the 3D inverted pendulum in Cartesian coordinates is given as follows.

$$m\begin{pmatrix} \ddot{x} \\ \ddot{y} \\ \ddot{z} \end{pmatrix} = (\mathrm{J}^{\mathrm{T}})^{-1}\begin{pmatrix} \tau_r \\ \tau_p \\ f \end{pmatrix} + \begin{pmatrix} 0 \\ 0 \\ -mg \end{pmatrix} \tag{4}$$

where m is the mass of the pendulum and g is gravity acceleration. The structure of the Jacobian J is

$$\mathrm{J} = \frac{\partial \boldsymbol{p}}{\partial \boldsymbol{q}} = \begin{pmatrix} 0 & rC_p & S_p \\ -rC_r & 0 & -S_r \\ -rC_rS_r/D & -rC_pS_p/D & D \end{pmatrix}. \tag{5}$$

$$C_r \equiv \cos\theta_r, C_p \equiv \cos\theta_p$$

To erase the inversed Jacobian that appears in (4), let us multiply the matrix J^{T} from the left.

$$m\begin{pmatrix} 0 & -rC_r & -rC_rS_r/D \\ rC_p & 0 & -rC_pS_p/D \\ S_p & -S_r & D \end{pmatrix}\begin{pmatrix} \ddot{x} \\ \ddot{y} \\ \ddot{z} \end{pmatrix} = \begin{pmatrix} \tau_r \\ \tau_p \\ f \end{pmatrix} - mg\begin{pmatrix} -rC_rS_r \\ -rC_pS_p/D \\ D \end{pmatrix}. \tag{6}$$

Using the first row of this equation and multiplying D/C_r we get

$$m(-rD\ddot{y} - rS_r\ddot{z}) = \frac{D}{C_r}\tau_r + rS_rmg. \tag{7}$$

By substituting kinematic relationship of equations (2) and (3), we get a good-looking equation that describes the dynamics along the y-axis.

$$m(-z\ddot{y} + y\ddot{z}) = \frac{D}{C_r}\tau_r - mgy \tag{8}$$

A similar procedure for the second row of (6) yields the equation for the dynamics along the x-axis.

$$m(z\ddot{x} - x\ddot{z}) = \frac{D}{C_p}\tau_p + mgx \tag{9}$$

3.2 3D Linear Inverted Pendulum Mode

Although the moving pattern of the pendulum has vast possibilities, we wanted to select a class of motion which would be suitable for walking. For this reason, we apply constraints to limit the motion of the pendulum. The first constraint limits the motion in a plane with given normal vector $(k_x, k_y, -1)$ and z intersection z_c.

$$z = k_x x + k_y y + z_c \tag{10}$$

For a walking robot, the normal vector should match the slope of the ground and the z intersection should be the average distance of the center of the robot's mass from the ground. In further calculation, we prepare the second derivatives of (10).

$$\ddot{z} = k_x\ddot{x} + k_y\ddot{y} \tag{11}$$

Substituting these constraints into equations (8) and (9), we will obtain the dynamics of the pendulum under the constraints. From a straightforward calculation we obtain

$$\ddot{y} = \frac{g}{z_c}y - \frac{k_1}{z_c}(x\ddot{y} - \ddot{x}y) - \frac{1}{mz_c}u_r \tag{12}$$
$$\ddot{x} = \frac{g}{z_c}x + \frac{k_2}{z_c}(x\ddot{y} - \ddot{x}y) + \frac{1}{mz_c}u_p \tag{13}$$

where u_r, u_p are new virtual inputs which are introduced to compensate input nonlinearity.

$$\tau_r = \frac{C_r}{D}u_r \tag{14}$$
$$\tau_p = \frac{C_p}{D}u_p \tag{15}$$

In the case of the walking on a flat plane, we can set the horizontal constraint plane ($k_x = 0, k_y = 0$) and we get

$$\ddot{y} = \frac{g}{z_c} y - \frac{1}{m z_c} u_r \tag{16}$$

$$\ddot{x} = \frac{g}{z_c} x + \frac{1}{m z_c} u_p. \tag{17}$$

In the case of the walking on a slope or a stairs where $k_x, k_y \neq 0$, we need another constraint. From $x\times(12)+y\times(13)$ we obtain

$$x\ddot{y} - \ddot{x}y = \frac{-1}{mz}(u_r x + u_p y). \tag{18}$$

Therefore, we obtain the dynamics of (16) and (17) in the case of an inclined constraint plane by introducing the following new constraint about the inputs.

$$u_r x + u_p y = 0 \tag{19}$$

Equations (16) and (17) are independent linear equations. The only parameter which governs those dynamics is z_c, i.e., the z intersection of the constraint plane and the inclination of the plane never affect the horizontal motion. Note that the original dynamics were nonlinear and we derived linear dynamics without using any approximation.

Let us call this the Three-Dimensional Linear Inverted Pendulum Mode (3D-LIPM). The first author and Tani introduced a two-dimensional version of this dynamics mode [6] and Hara, Yokokawa and Sadao extended it to three dimensions in the case of zero input torque [4].

4 Control of lateral motion

The 3D-LIPM dynamics of equations (16) and (17) enables us to design a simple real-time controller for biped walking. In this paper, we treat a walking on a flat floor. This means that we do not have to take account of the input constraint (19) and we can completely separate controllers for sagittal and lateral motions.

In this section, we will explain the method for controlling stepping motion in the lateral plane (y-direction).

4.1 Ideal stepping pattern

Figures 4 and 5 describe an ideal stepping motion of a robot which follows the 3D-LIPM dynamics. We

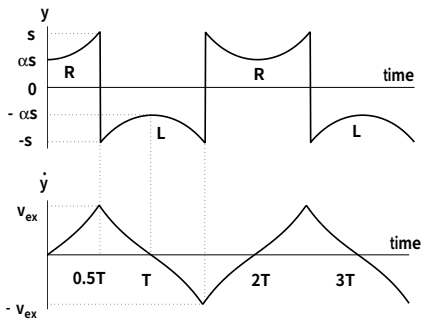

Figure 4: *Position and velocity of a robot's center of gravity when performing an ideal steady stepping motion. The stepping cycle is $2T$, the width of a step is $2s$. Parameter $\alpha(0 < \alpha < 1)$ specifies the position at the moment velocity changes its sign. The position jumps the distance of the step length at each support foot exchange, due to the change of origin shown in Figure 5.*

use 3D-LIPM (16) with zero input ($u_r = 0$) both in the right and the left support.

$$\ddot{y} = \frac{g}{z_c} y \tag{20}$$

Given the above dynamics, a trajectory of a particular support phase with an initial condition of $(y_i, \dot{y}_i)$ at time t_i can be calculated.

$$y(t) = y_i \cosh(\frac{t-t_i}{T_c}) + T_c \dot{y}_i \sinh(\frac{t-t_i}{T_c}) \tag{21}$$

$$\dot{y}(t) = \frac{y_i}{T_c} \sinh(\frac{t-t_i}{T_c}) + \dot{y}_i \cosh(\frac{t-t_i}{T_c}) \tag{22}$$

$$T_c \equiv \sqrt{z_c/g}$$

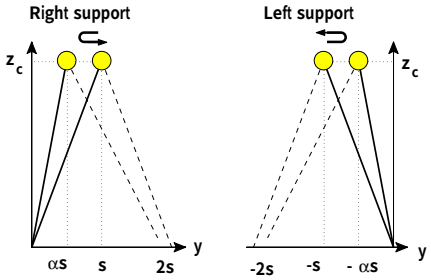

Figure 5: *Motion of the inverted pendulum corresponding to Figure 4*

In this stepping pattern, we assume that the exchange of the support leg occurs instantaneously, and

the velocity of the center of gravity is passed without loss from the end of last support to the start of new support.

Let us derive the relationship between the cycle and the geometry of the stepping motion. From the trajectory in Figure 4 and (21), we get

$$s = \alpha s \cosh(\frac{T}{2T_c}). \tag{23}$$

Solving this about T, we obtain the half cycle of stepping motion.

$$T = 2T_c \ln(\frac{1+\sqrt{1-\alpha^2}}{\alpha}) \tag{24}$$

This equation describes that when the body swing becomes small ($\alpha \to 1$) the stepping period becomes short ($T \to 0$). Conversely, when the body swing becomes large ($\alpha \to 0$) the stepping period becomes long ($T \to \infty$). This nature of stepping motion can be understood intuitively by imaging a boll rolling between two potentials as shown in Figure 6.

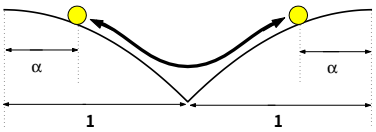

Figure 6: *A ball rolling between two potentials*

4.2 Lateral control of Meltran V

As the basic requirement for ideal stepping motion, constraint control to a horizontal plane is applied to Meltran V to realize 3D-LIPM dynamics, i.e., the control of the prismatic joint of the support leg so that the center of the hip joint moves in a constraint plane. At the same time, the body posture is also controlled to keep the robot's body upright. We do not apply the input constraint (19) since it is not neccessary when we use the horizontal constraint plane.

We implemented these controls based on the resolved motion rate control [13] that uses an inverse Jacobian to calculate joint speed references. With these controls, we can expect to approximately realize the 3D-LIPM because Meltran V was designed to have lightweight feet and good mass concentration around the center of the hip joints.

Even the constraint control works well, though there are still problems in realizing the ideal stepping motion by the actual robot. First, the actual robot in a single-support phase does not follow the ideal 3D-LIPM of equation (20) unless proper feedback control is applied, because there exist parameter errors and the real robot has more complicated dynamics which are not modeled by the 3D-LIPM. To clear these problems we introduce following feedback.

$$u_r = \mathrm{sign}(\dot{y}) k_E (E_{ref} - E) \tag{25}$$

$$E \equiv -\frac{g}{2z_c} y^2 + \frac{1}{2}\dot{y}^2 \tag{26}$$

$$E_{ref} \equiv -\frac{g}{2z_c}(\alpha s)^2 \tag{27}$$

The function $\mathrm{sign}(x)$ returns $+1$ or -1 depending the sign of x. k_E is a feedback gain taking a positive value which should be tuned by experiments. A torque feedback controller using a foot force sensor drives the foot actuator to generate torque u_r.

We call the quantity E *the orbital energy* because it has a dimension of energy per unit mass. Differentiating E by time we obtain

$$\dot{E} = -\frac{g}{z_c} y\dot{y} + \dot{y}\ddot{y}. \tag{28}$$

When we substitute the ideal dynamics of equation (20) into this equation we obtain $\dot{E} = 0$. Therefore, E will be kept constant as long as the robot's motion is ideal. When we substitute the 3D-LIPM dynamics of equation (16) and the control law of equation (25) into equation (28) we see how the orbital energy will behave under the proposed control law.

$$\dot{E} = \frac{1}{mz_c} |\dot{y}| k_E (E_{ref} - E) \tag{29}$$

From this equation we can see E will be controlled to specified constant value E_{ref}. A similar control method was proposed by Fujimoto and Kawamura to control a humanoid robot in a computer simulation[2].

The second problem concerns the body speed at the instant of support leg exchange. Although we assumed the speed at the end of one cycle to be equal to the initial speed of the new cycle in ideal stepping motion, this does not happen in real-world circumstances. Due to the complicated impact dynamics and internal vibration of the mechanism, the initial speed just after support exchange is difficult to predict.

To cope with this uncertainty, we insert a double-support state between successive support phases (Figure 7). After touchdown of the swing foot, the robot body travels the distance $2\beta s$ keeping both feet on the

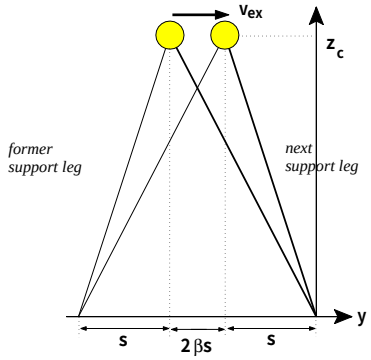

Figure 7: *For reliable support leg exchange, a double-leg support phase was inserted. The robot body travels the distance $2\beta s$ with both feet on the ground in the period between each single-leg support phase.*

ground, then starts a new support phase by lifting up the previous support leg. We can control the body speed of the robot in the double-support phase by a simple torque control[10]. For the target speed of this control, we use v_{ex} which is the speed at the support leg exchange in ideal stepping motion. It is calculated from (22).

$$v_{ex} = \frac{\alpha s}{T_c} \sinh(\frac{T}{2T_c}) \tag{30}$$

To detect good timing for starting the next single-support phase, the robot calculates the orbital energy E about the next support leg during the double-support phase. At the moment E reaches E_{ref}, the robot starts the new single support motion by lifting up the previous support leg. This way we can guarantee that each single-support phase will start with the specified orbital energy E_{ref} even the speed control in the double-support period did not work well.

We applied above control algorithm to Meltran V and it achieved a stepping motion of good reliability. Figure 8 shows the data of position and velocity, and Figure 9 shows the orbital energy and the roll moment of the feet which corresponds to u_r in equation (25). In those plots, we placed the origin at the center of the robot's body at all times instead of swapping the origin on the supporting condition as in Figure 5. The body center coordinate allows us to apply the leg control consistently. When a foot is in the support phase, its position (velocity) in the body coordinate corresponds to the body position (velocity) with respect to the support foot by reversing its sign.

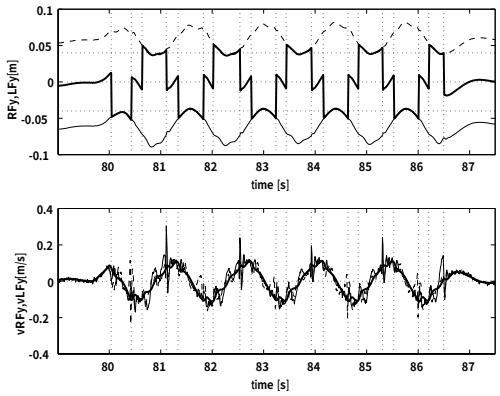

Figure 8: *Experiment of steady stepping motion. The vertical dotted lines indicate the time of the supporting mode change. The upper plot is the position of the feet with respect to the center of the body. The thin solid line is the right foot, the dashed line is the left foot and the thick line indicates the supporting foot. The robot is in double-support phase when the thick line runs in the middle of the feet trajectories. The lower plot is the velocity of the feet with respect to the center of the body. The thick line indicates the supporting foot velocity which is associated with body speed. A Kalman filter was used to obtain smooth data by attenuating high-frequency noise.*

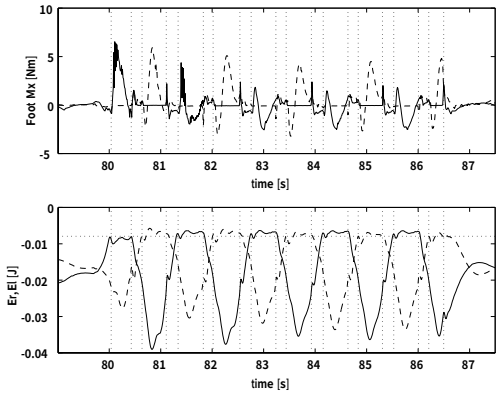

Figure 9: *Data of the same experiment shown in Figure 8. The upper plot is the moment around x-axis. The lower plot is the orbital energy. The horizontal dotted line shows the reference energy E_{ref}. The vertical dotted lines in both plots indicate the time of supporting mode change.*

5 Control of sagittal motion

Figure 10 illustrates successive steps in the sagittal plane (x-direction). For the reference dynamics of each support phase (B→D, D'→F), we adopt the 3D-LIPM (17) with zero input as we did for the lateral motion.

$$\ddot{x} = \frac{g}{z_c} x \tag{31}$$

Since the robot is controlled to continue a steady stepping motion whose support time is T, the initial body state $(x_i^{(n)}, v_i^{(n)})$ and the final body state $(x_f^{(n)}, v_f^{(n)})$ have the following relationship.

$$\begin{pmatrix} x_f^{(n)} \\ v_f^{(n)} \end{pmatrix} = \begin{pmatrix} C_T & T_c S_T \\ S_T/T_c & C_T \end{pmatrix} \begin{pmatrix} x_i^{(n)} \\ v_i^{(n)} \end{pmatrix} \tag{32}$$

$$C_T \equiv \cosh(T/T_c), S_T \equiv \sinh(T/T_c)$$

To change the walking speed, we must change the foothold (point E) to modify the initial condition of the support phase (D'→F). When the desired status at the end of support (point F) is given as (x_d, v_d) we can define error norm with certain weight $a, b > 0$ as

$$N \equiv a(x_d - x_f^{(2)})^2 + b(v_d - v_f^{(2)})^2.$$

By substituting (32) into this equation and calculating the foothold of $x_i^{(2)}$ which minimize N, we obtain a proper control law.

$$x_i^{(2)} = (aC_T(x_d - S_T T_c v_d) + bS_T/T_c(v_d - C_T v_f))/D_T \tag{33}$$

$$D_T \equiv aC_T^2 + b(S_T/T_c)^2$$

To determine the foothold E we also need the distance that body travels in the double support. The distance is calculated as

$$d = v_f^{(1)} \frac{2\beta s}{v_{ex}}. \tag{34}$$

The motion of the support leg is controlled to follow the ideal trajectory of equation (31) using a simple PD feedback law whose output is u_p in equation (15). The motion of the swing leg is controlled to arrive at the point E at the expected touchdown time (dashed curve from A to E in Figure 10).

Figure 11 plots sagittal motion data of 3D walking performed by the Meltran V robot. In this experiment, the robot walked 6 steps forward. The period of support was controlled to 0.55 s and the maximum step length was 0.15 m.

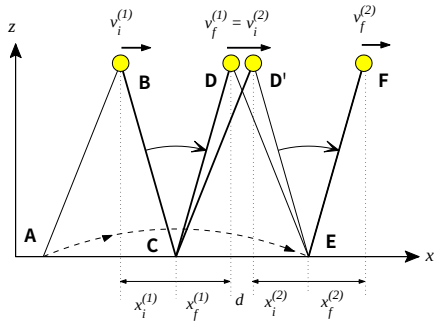

Figure 10: *Two successive steps in the sagittal plane are illustrated. The body travels from B to D in the single-leg support phase, then moves from D to D' in the double-leg support phase with constant speed $v_f^{(1)}$, and then travels D' to F in the second single-support phase. While the body moves from B to D, the tip of the swing leg travels from A to E (dashed curved line). By changing the position of E we can control the final body speed $v_f^{(2)}$ at the point F. Except for our inserted double-support phase, this is the same idea proposed by Miura and Shimoyama [7].*

6 Summary and Conclusions

In this paper we introduced the Meltran V, our new biped walking robot with telescopic legs. To control the robot, we derived the Three-Dimensional Linear Inverted Pendulum Mode (3D-LIPM) which is useful for real-time walking control in a 3D space. We discussed a method for controlling steady lateral stepping motion and explained our method of 3D walking control. Meltran V could walk successfully with our proposed algorithm.

In this paper we only demonstrated a walk on a flat floor, however the 3D-LIPM model can be used for walking over rugged terrain. That will be the subject of our next report.

References

[1] Dunn, Eric.R and Howe, Robert D., "Foot Placement and Velocity Control in Smooth Bipedal Walking," Proc. of 1996 ICRA, pp.578-583, 1996.

[2] Fujimoto, Y. and Kawamura, A., "Three Dimensional Digital Simulation and Autonomous Walking Control for Eight-Axis Bipd Robot," Proc. of the 1995 ICRA, pp.2877-2884, 1995.

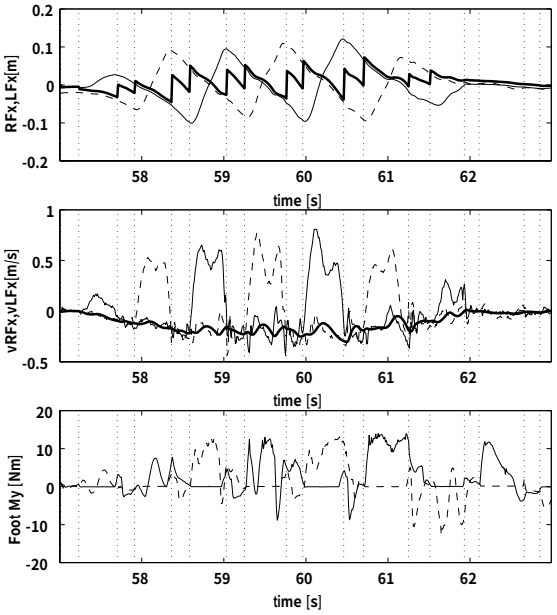

Figure 11: *Sagittal motion data of Meltran V's 3D walking. The upper plot is the position of the feet with respect to the center of the body. The thin solid line is the right foot, the dashed line is the left foot, and the thick line indicates the supporting foot. In the period that thick line runs in the middle of the feet trajectories, the robot is in double-support phase. The middle plot is the velocity of the feet with respect to the body center. The thick line indicates the supporting foot velocity which corresponds to negative body speed. The bottom plot is the foot pitch moment which is generated to control the body motion.*

[3] Grishin,A, et.al, "Dynamic Walking of a Vehicle With Two Telescopic Legs Controlled by Two Drives," The International Journal of Robotics Research, Vol.13, No.2, pp.137-147, 1994.

[4] Hara,K., Yokokawa,R. and Sadao, K., "Dynamic Control of Biped Locomotion Robot for Disturbance on Lateral Plane," Proc. of The Japan Society of Mechanical Engineers 72nd kansai meeting, pp.10-37–10-38, 1997 (in Japanese).

[5] Hirai, K., Hirose,M., Haikawa, Y. and Takenaka, T., "The Development of Honda Humanoid Robot," Proc. of the 1998 ICRA, pp.1321-1326, 1998.

[6] Kajita,S. and Tani, K., "Study of Dynamic Biped Locomotion on Rugged Terrain," Proc. of the 1991 ICRA, pp.1405-1410, 1991.

[7] Miura,H. and Shimoyama, I., "Dynamic walk of a biped," International Jurnal of Robotics Research, Vol.3, No.2, pp.60-72, 1984.

[8] Katoh,R. and Mori,M.,"Control method of biped locomotion giving asymptotic stability of trajectory," Automatica, Vol.20, No.4, pp.405-414, 1984.

[9] Playter, Robert R. and Raibert, Marc H., "Control of a Biped Somersault in 3D," Proc. of IFToMM-jc International Symposium on Theory of Machines and Mechanisms (in Nagoya, Japan), pp.669-674, 1992.

[10] Pratt, J., Dilworth, P. and Pratt, G., "Virtual Model Control of a Bipedal Walking Robot," Proc. of the 1997 ICRA, pp.193-198, 1997.

[11] Shih, Ching-Long., "Analysis of the Dynamics of a Biped Robot with Seven Degrees of Freedom," Proc. of the 1996 ICRA, pp.3008-3013, 1996.

[12] Yamaguchi, J.,Soga,E., Inoue, S. and Takanishi, A., "Development of a Bipedal Humanoid Robot – Control Method of Whole Body Cooperative Dynamic Biped Walking –," Proc. of the 1999 ICRA, pp.368-374, 1999.

[13] Whitney,D., "Resolved Motion Rate Control of Manupulators and Human Prostheses," IEEE Transactions on man-machine systems, vol.MMS-10, no.2, 1969.